Characteristics of ionospheric irregularities during geomagnetic storms using long-term worldwide GNSS data

Takuya Sori[1], Atsuki Shinbori[2], Yuichi Otsuka[2], Michi Nishioka[3], and Septi Perwitasari[3]

[1]Research Institute for Sustainable Humanosphere, Kyoto University, Kyoto, Japan.
[2]Institute for Space-Earth Environmental Research, Nagoya University, Nagoya, Japan.
[3]National Institute of Information and Communications Technology, Koganei, Tokyo, Japan.

June 11, 2024 (13:30 ~)

Introduction

Coronal mass ejections (CME) and Corotating interaction regions (CIR) cause a geomagnetic storm

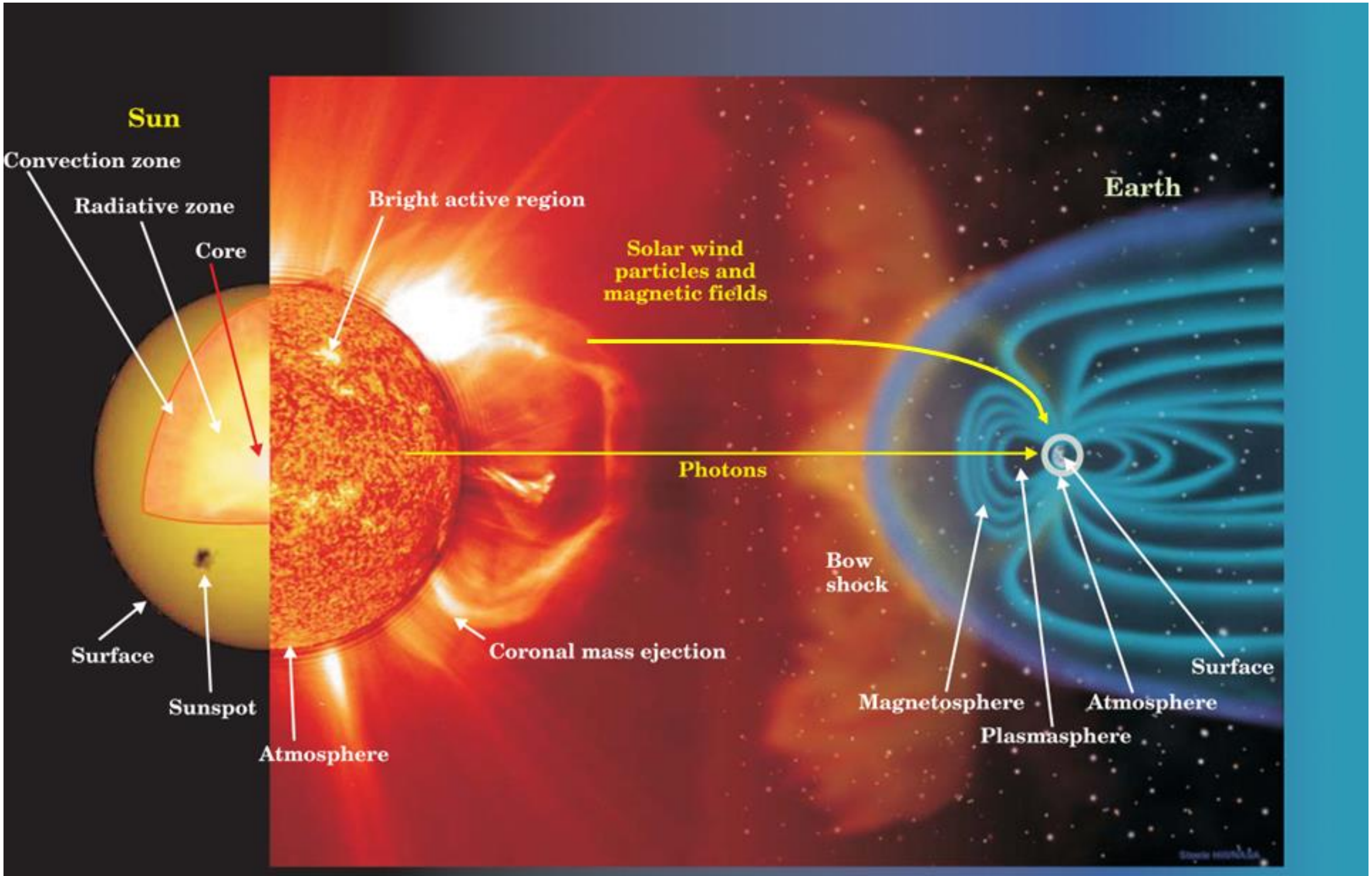

[modified Lean, 2005]

Introduction

Ionosphere affects radio propagation

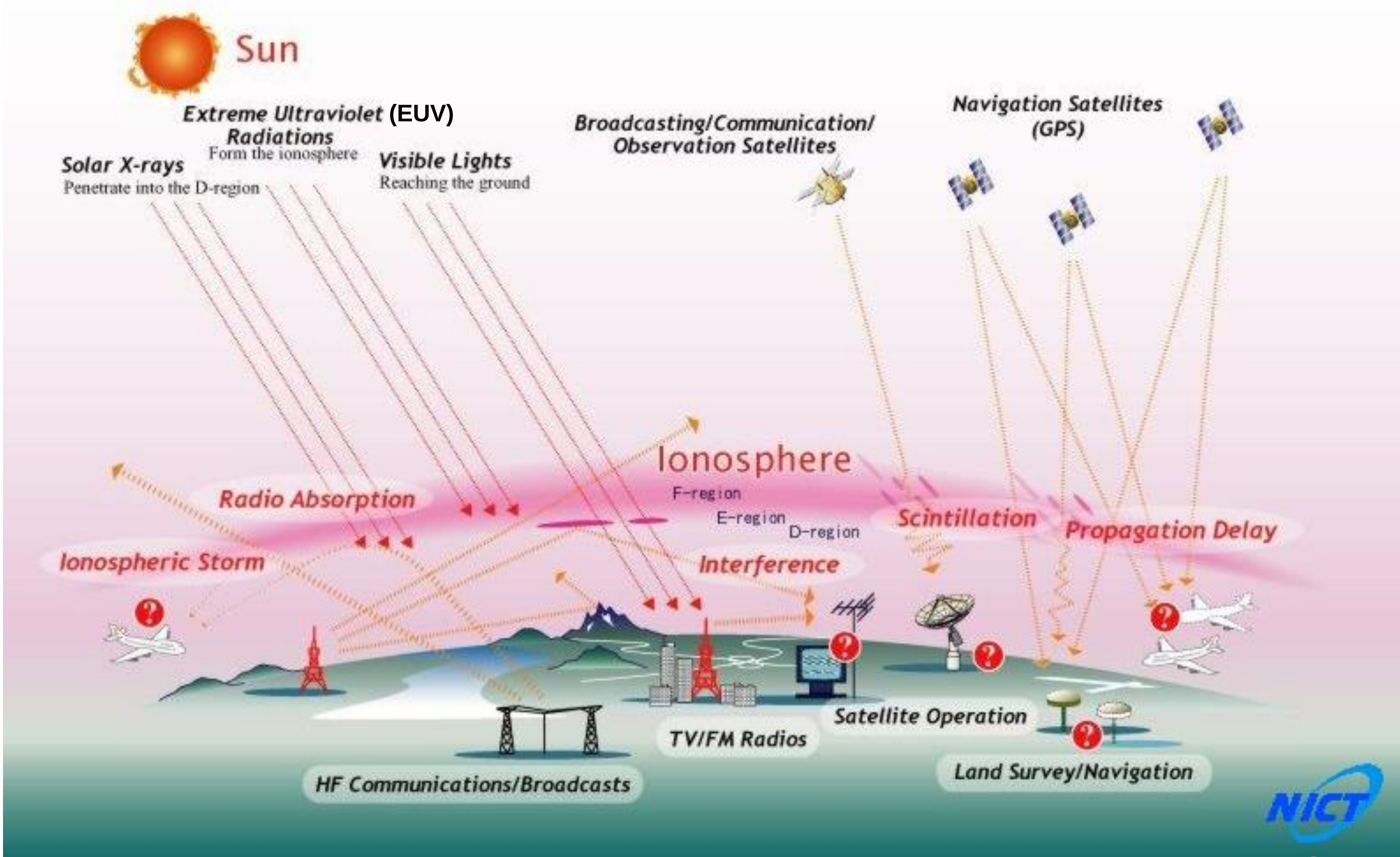

(https://wdc.nict.go.jp/IONO/index_E.html)

Introduction

Ionosphere affects radio propagation

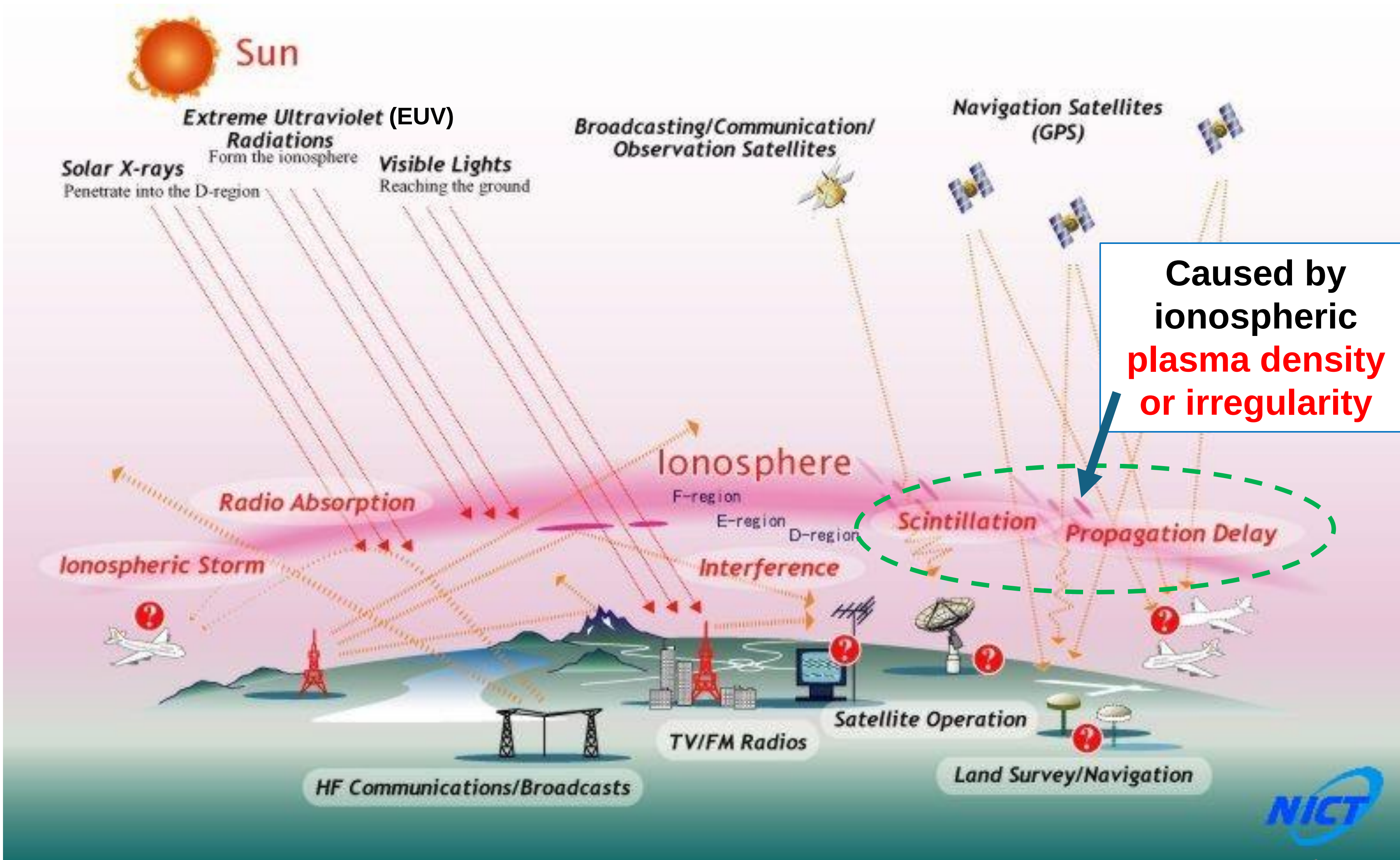

(https://wdc.nict.go.jp/IONO/index_E.html)

Introduction

Ionospheric plasma density variations are caused by various reasons (earthquake, volcanic eruption, solar eclipse, solar flare, geomagnetic storm, etc..)

Geomagnetic storm effects on our daily life

Positioning error

Starlink satellites lost

Electric power systems broken

(https://www.nhk.or.jp/ashitanavi/article/9506.html)

Introduction

We need to study characteristics of ionospheric response during geomagnetic storms

Geomagnetic storm effects on our daily life

Positioning error

Starlink satellites lost

Electric power systems broken

(https://www.nhk.or.jp/ashitanavi/article/9506.html)

Motivation

Clarify the effects of the CME and CIR storms on the high-latitude ionosphere (auroral oval) using global GNSS data

Datasets

- SYM-H index data are provided by WDC, Kyoto University (http://wdc.kugi.kyoto-u.ac.jp/index.html).
- Solar wind and IMF data are provided by the Coordinated Data Analysis Web (CDAWeb), NASA (https://cdaweb.gsfc.nasa.gov/).
- Global GNSS data are provided by the ISEE, Nagoya University (https://stdb2.isee.nagoya-u.ac.jp/GPS/GPS-TEC/).

Analysis method

Brief description of the Rate of TEC Index (ROTI)

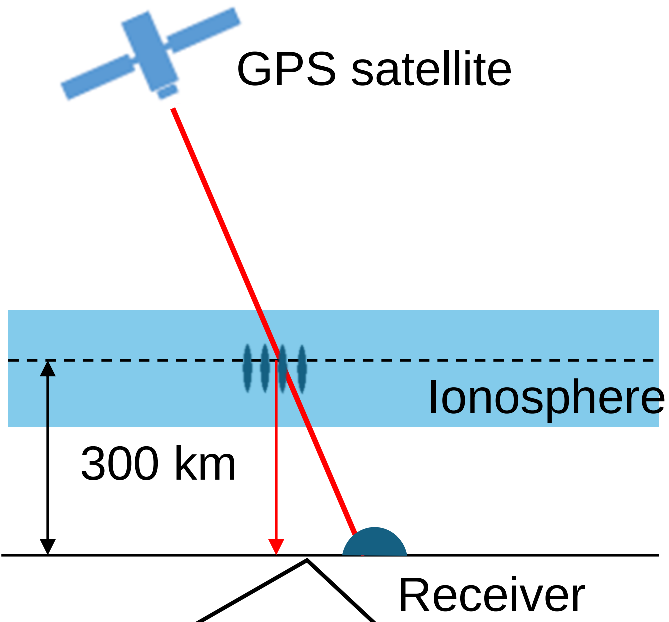

We mapped the TEC and ROTI at a height of 300 km in the thin-layer ionosphere.

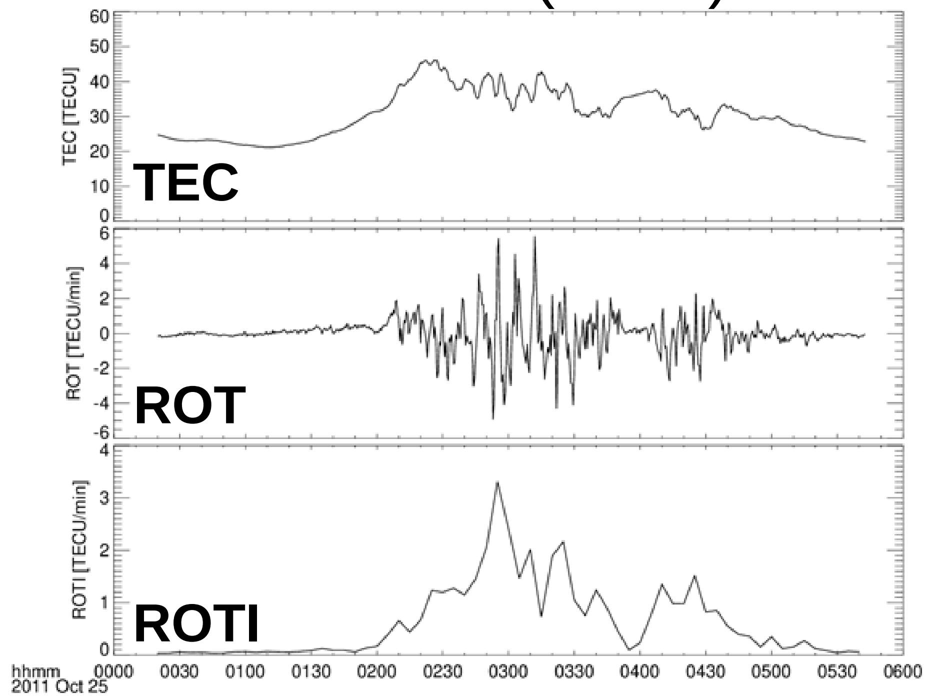

TEC, ROT and ROTI observed at the point of the GPS receiver (28°N, 278°E) (2011.10.25/00:00–06:00 UT)

Calculation method of ROTI with GNSS-TEC data

$$\mathrm{ROT} = \frac{\mathrm{T}\,(\mathrm{t}_0+0.5)-\mathrm{T}\,(\mathrm{t}_0)}{0.5}\ [\mathrm{TECU/min}]$$

$\mathrm{T}\,(\mathrm{t})\ [\mathrm{TECU}]$: TEC at time t
($[\mathrm{TECU}] = [10^{16}/\mathrm{m}^2]$)

$$\mathrm{ROTI} = \sqrt{\langle \mathrm{ROT}^2 \rangle - \langle \mathrm{ROT} \rangle^2}\ [\mathrm{TECU/min}]$$

[Pi et al., 1997]

What can ROTI values detect?

- **Auroral region (auroral oval)**

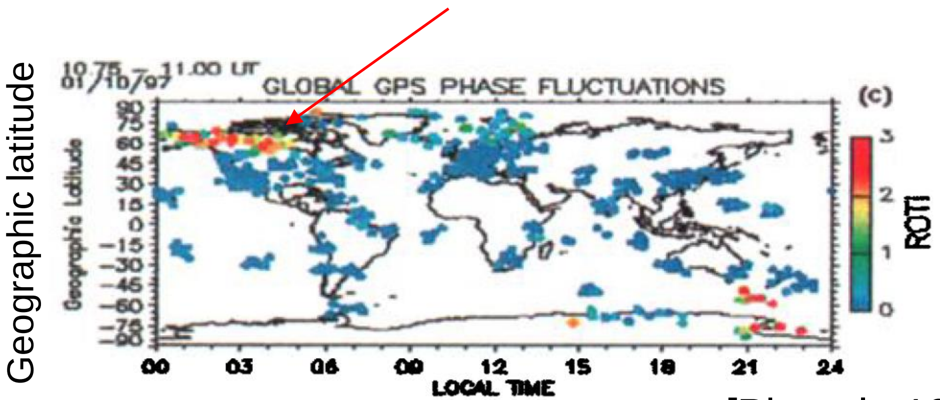

Ionospheric irregularities in the high latitudes due to **particle precipitation** and **dynamical processes including high speed plasma convection**

[Pi et al., 1997]

- **Equatorial–low latitude regions (plasma bubble)**

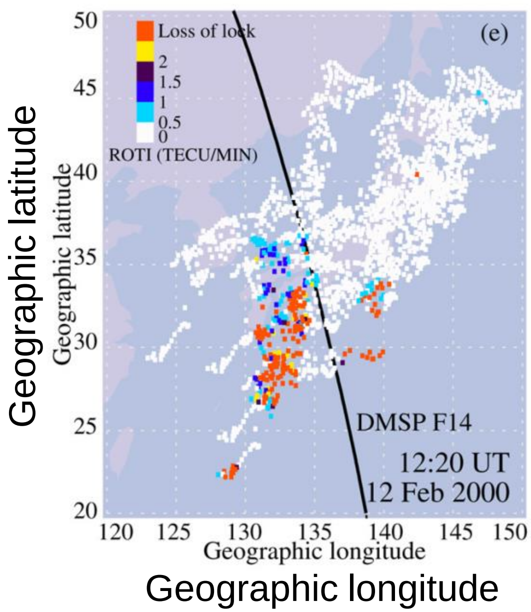

Ionospheric irregularities in the equatorial and low latitudes due to **plasma bubbles generated by the Rayleigh-Taylor instability mechanism**

[Ma and Maruyama, 2006]

What can ROTI values detect?

- **Auroral region (auroral oval)**

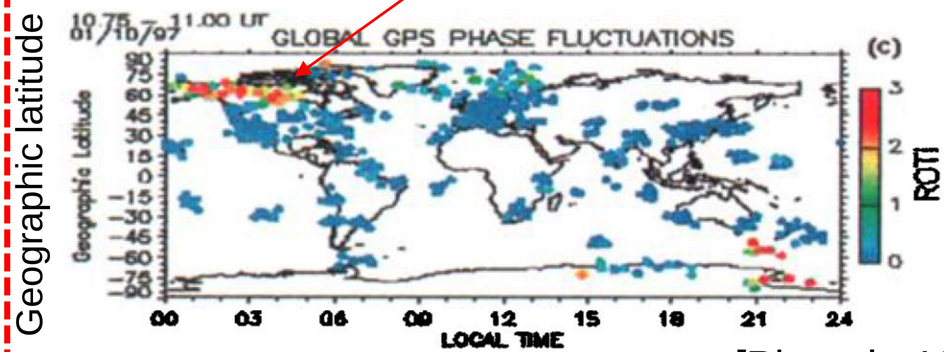

Ionospheric irregularities in the high latitudes due to **particle precipitation** and **dynamical processes including high speed plasma convection**

[Pi et al., 1997]

- **Equatorial–low latitude regions (plasma bubble)**

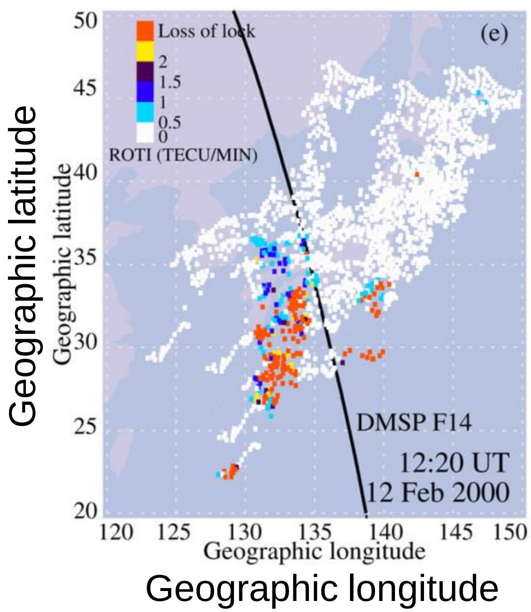

Ionospheric irregularities in the equatorial and low latitudes due to **plasma bubbles generated by the Rayleigh-Taylor instability mechanism**

[Ma and Maruyama, 2006]

Analysis method

Analysis period	1/1/2000～12/31/2018 (19 years)
Definition of <u>geomagnetic storm events</u>	SYM-H variations with the minimum value of less than -40 nT
The number of events	**653** (CME: 317 events, CIR: 336 events)

We investigate the relationship between temporal and spatial variations of the ROTI and other parameters (solar wind and geomagnetic index) **using a superposed epoch analysis method**

(We define the time of the SYM-H minimum as a zero epoch time)

Results

Epoch analysis results of solar wind parameter and geomagnetic index

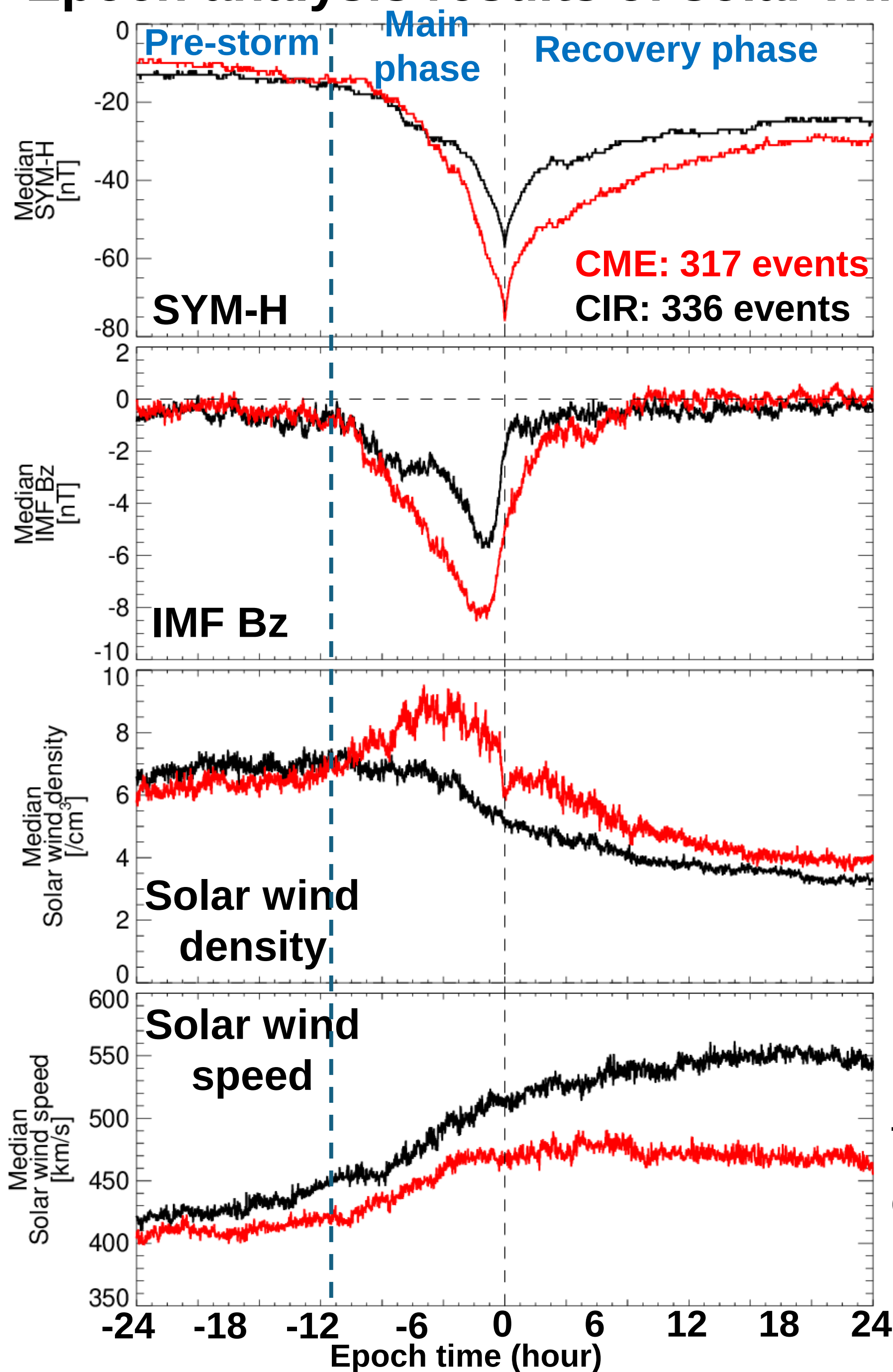

CIR > CME

CIR > CME

CME > CIR

The median solar wind density for the CIR events peaked earlier than that for the CME events.

CIR > CME

The median solar wind speed for the CIR events peaked during the storm recovery phase.

Spatiotemporal variations of median ROTI at high latitudes

CME: 317 events **CIR: 336 events**

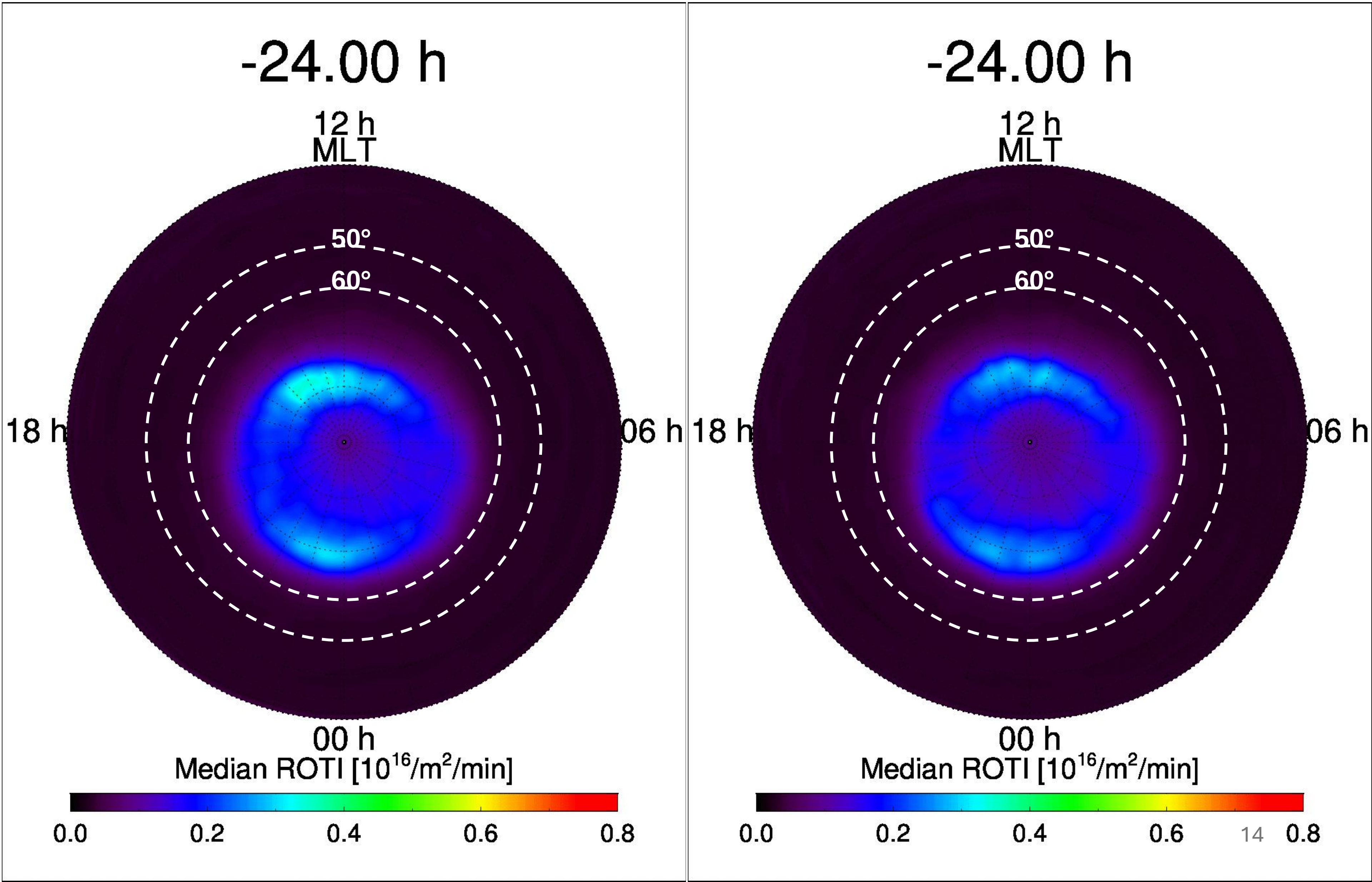

GMLAT–time plot of median ROTI at the specific MLTs

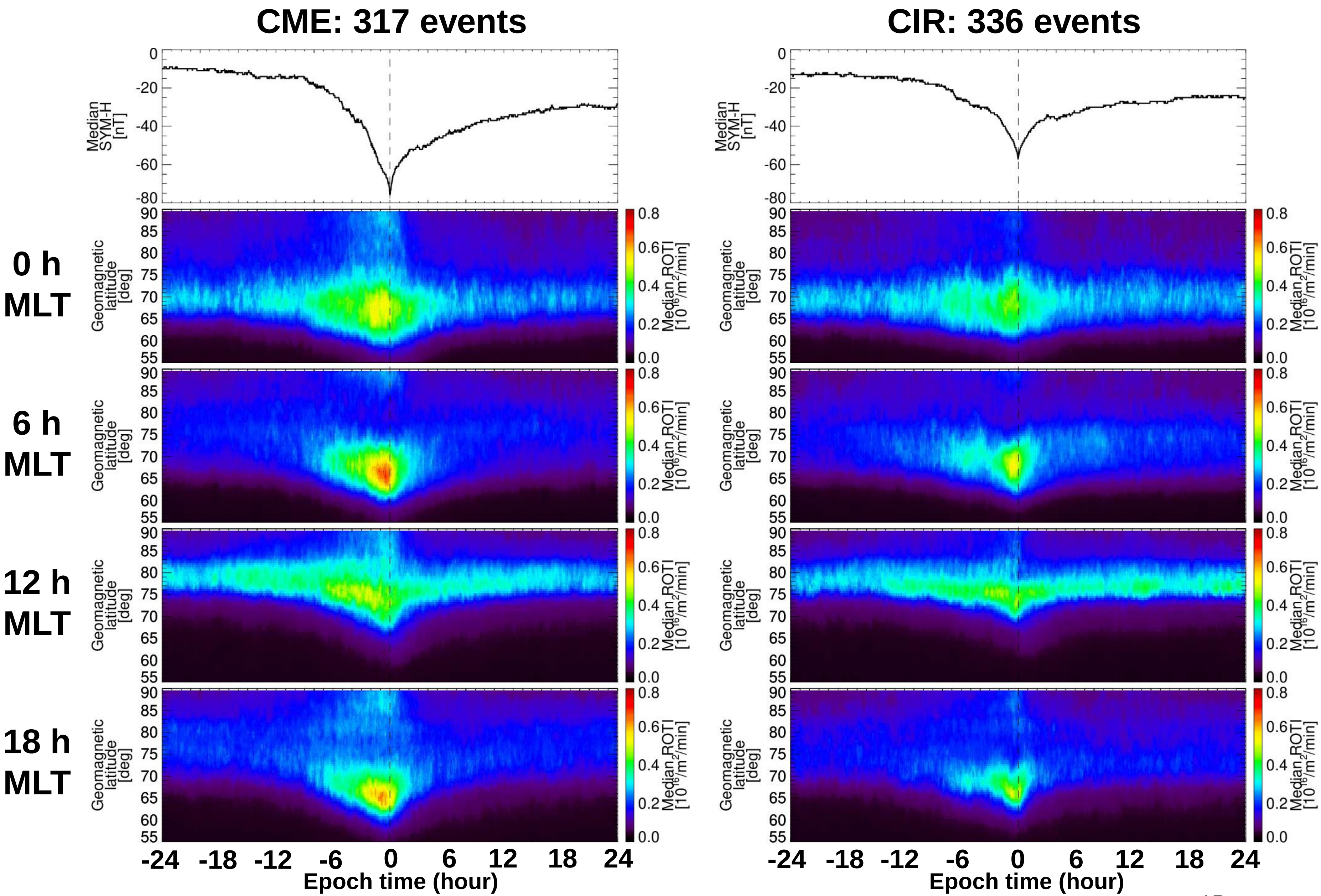

GMLAT–time plot of median ROTI at the specific MLTs

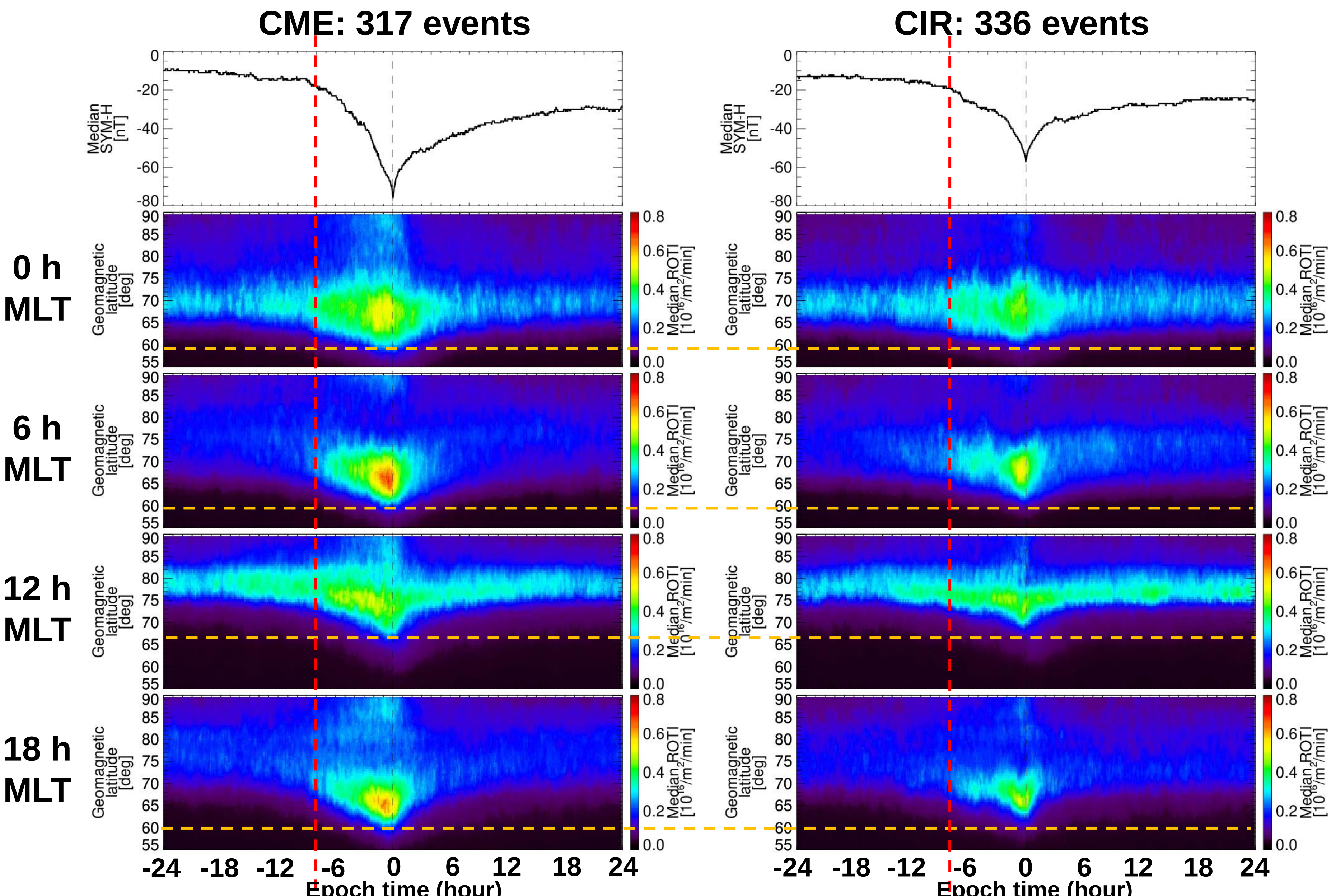

Summary and Discussion

IMF and solar wind parameters

The magnitudes of the IMF Bz and solar wind density was **larger** during the **CME-driven** storms than during the **CIR-driven** storms.

The magnitude of the solar wind speed was **smaller** during the **CME-driven** storms than during the **CIR-driven** storms.

SYM-H index

It is **larger** during the **CME-driven** storms than during the **CIR-driven** storms.

Superposed epoch analysis results for CME and CIR (previous study)

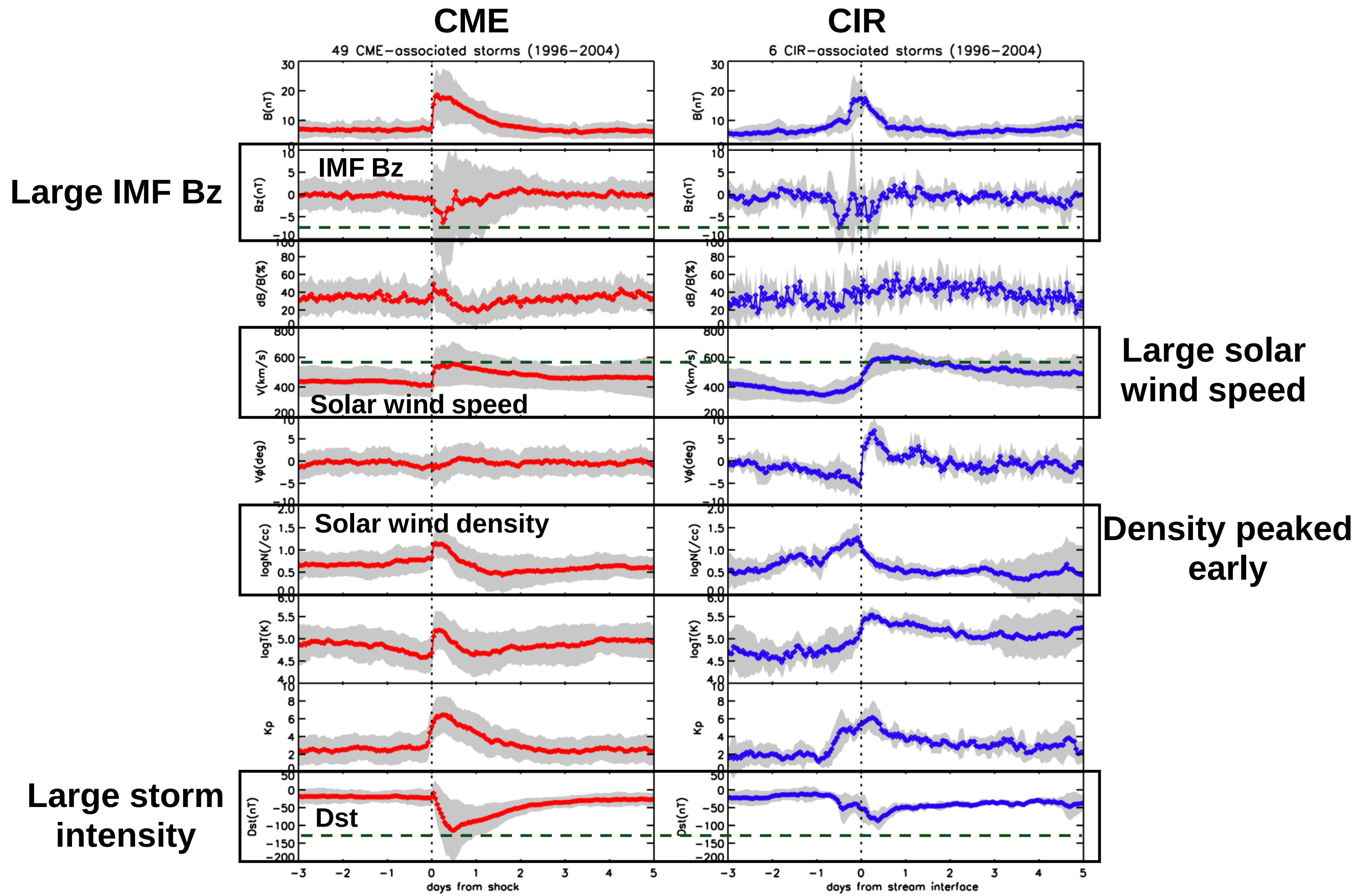

[Kataoka and Miyoshi, 2006]

Summary and Discussion

IMF and solar wind parameters

The magnitudes of the IMF Bz and solar wind density was **larger** during the **CME-driven** storms than during the **CIR-driven** storms.

The magnitude of the solar wind speed was **smaller** during the **CME-driven** storms than during the **CIR-driven** storms.

SYM-H index

It is **larger** during the **CME-driven** storms than during the **CIR-driven** storms.

The statistical results for the CME and CIR events are consistent with the characteristics of the CME- and CIR-driven storms reported by the previous study.

Summary and Discussion

Auroral oval

The enhanced ROTI region at all MLTs extended to the **lower latitudes** for the **CME** events than for the **CIR** events.

The ROTI values in the auroral oval were **larger** for the **CME** events than for the **CIR** events.

➡ The CME-driven storms disturbed the high-latitude ionosphere compared with the CIR-driven storms.

The results imply that **the region where the radio waves for communication, positioning, and broadcasting could be affected by the geomagnetic storms extends from the high- to the mid-latitudes.**

Conclusions

We clarified the effects of the CME and CIR storms on the high-latitude ionosphere (auroral oval) using long-term global GNSS data from 2000 to 2018.

- The auroral oval extended to **the lower latitudes** during **the CME-driven** storms than that during **the CIR-driven** storms.
- The ROTI values in the auroral oval were **larger** during **the CME-driven** storms than during **the CIR-driven** storms.

The radio waves we use every day could be disturbed even at the mid-latitudes when the CME-driven and CIR-driven geomagnetic storms occur.

Therefore, it is important to predict when the CME and CIR will reach the Earth and how large they are.

Conclusions

We clarified the effects of the CME and CIR storms on the high-latitude ionosphere (auroral oval) using long-term global GNSS data from 2000 to 2018.

- The auroral oval extended to **the lower latitudes** during **the CME-driven** storms than that during **the CIR-driven** storms.

- The ROTI values in the auroral oval were **larger** during **the CME-driven** storms than during **the CIR-driven** storms.

The radio waves we use every day could be disturbed even at the mid-latitudes when the CME-driven and CIR-driven geomagnetic storms occur.

Therefore, it is important to predict when the CME and CIR will reach the Earth and how large they are.

On the other hand, the statistical results of ROTI were not consistent with the spatial variation of ROTI during the recent geomagnetic storm in May 2024.

Example: Auroral oval during the giant storm in May 2024

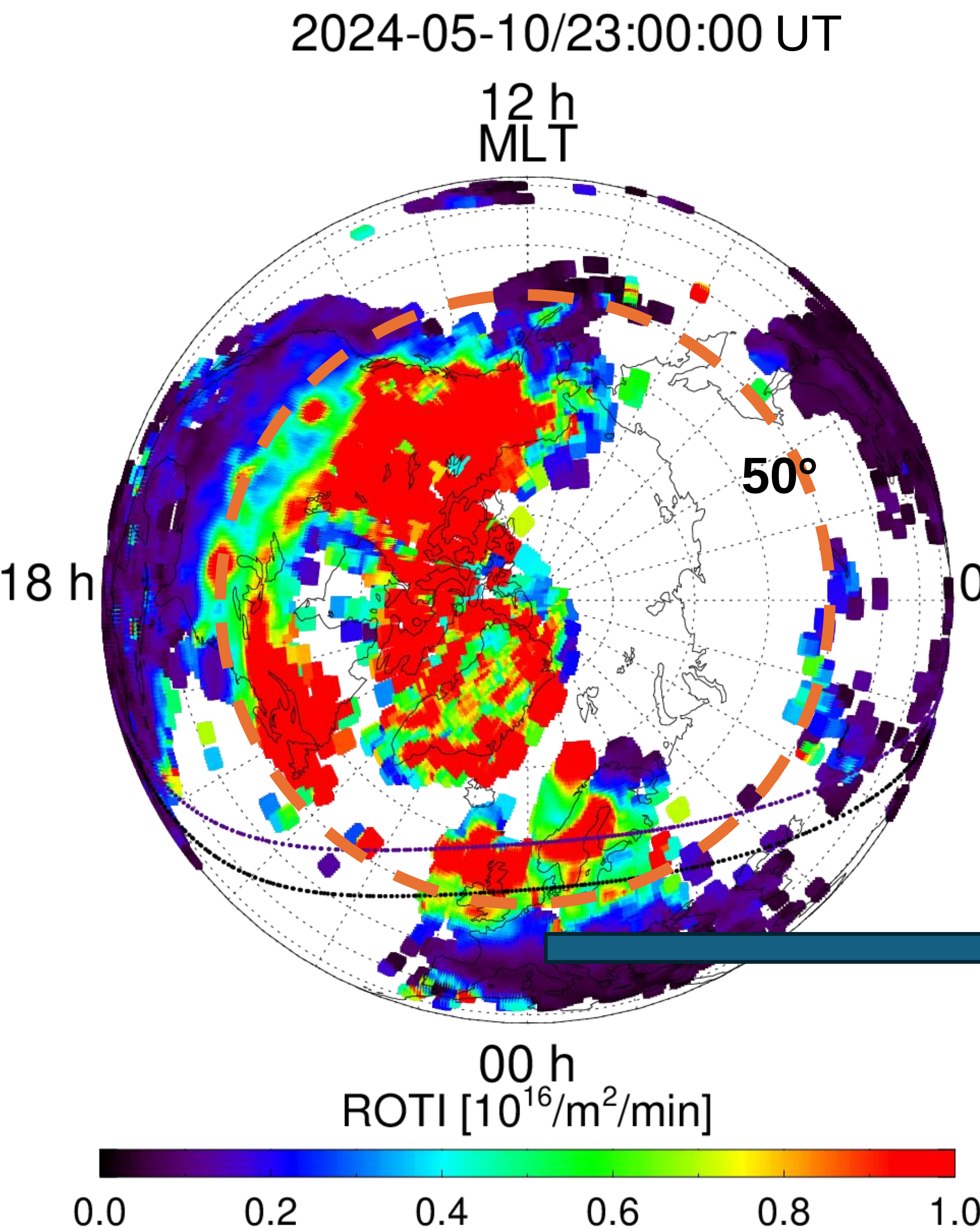

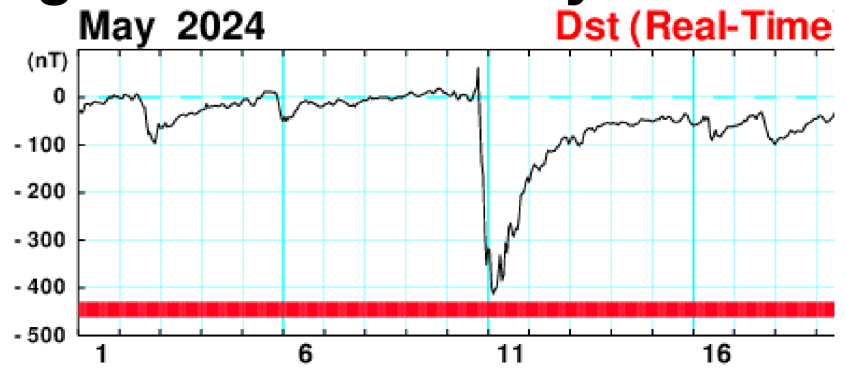

The equatorward edge of the auroral oval at midnight reached **< 50° N** in geomagnetic latitude.

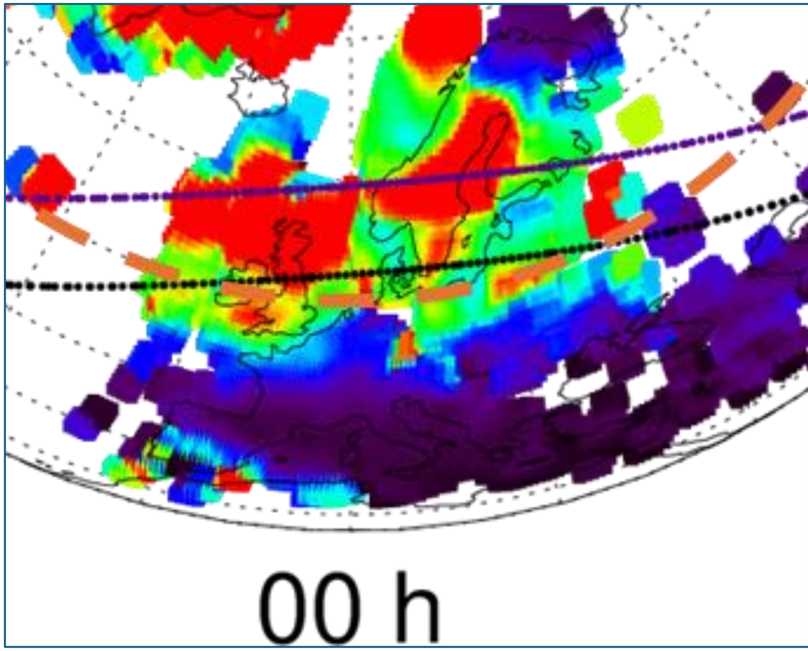

Example: Auroral oval during the giant storm in May 2024

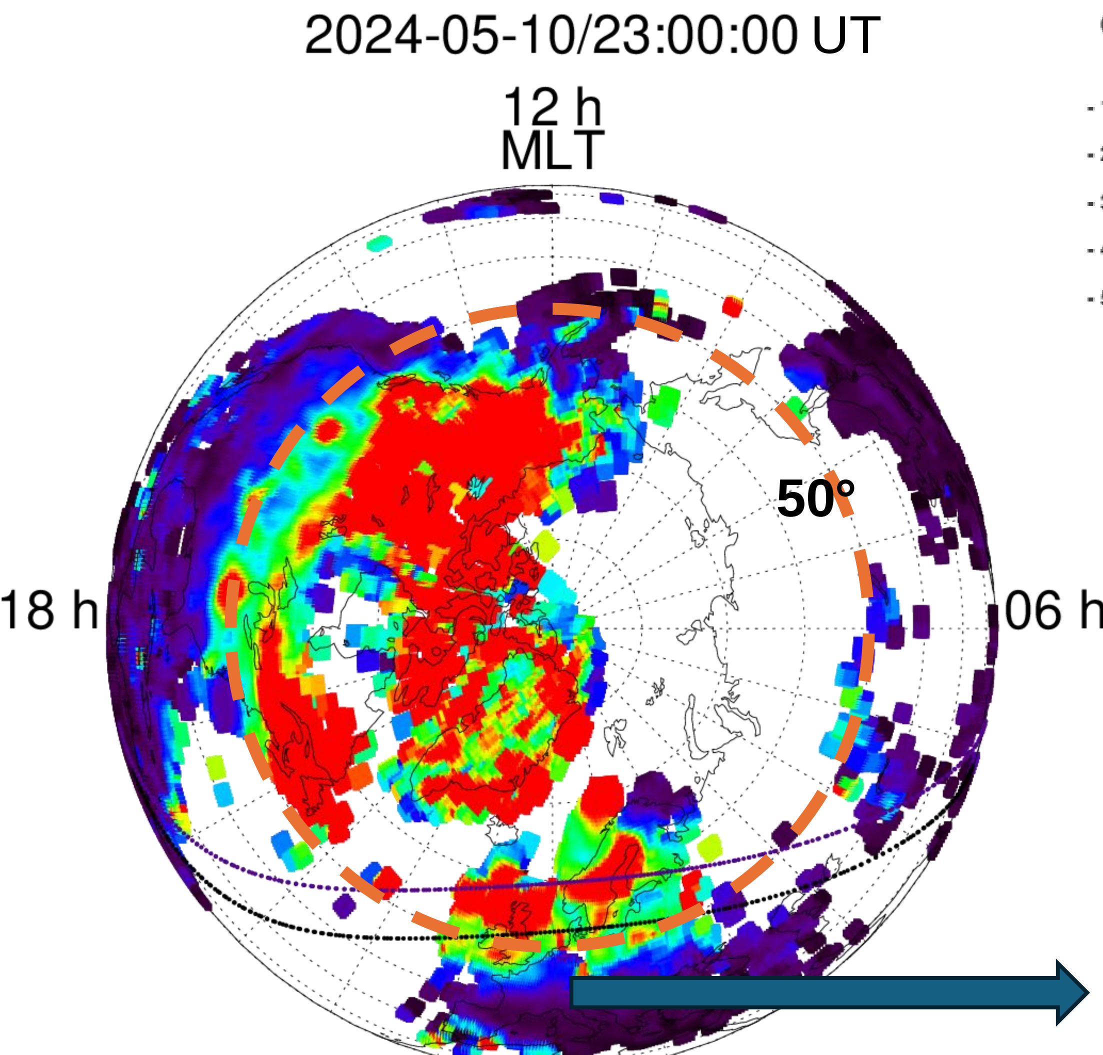

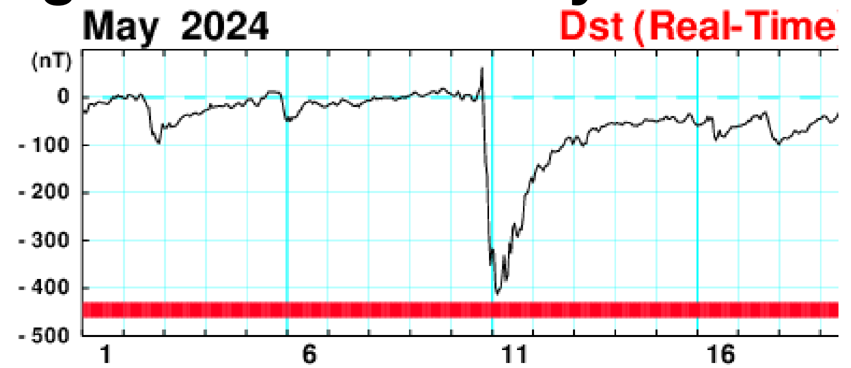

The equatorward edge of the auroral oval at midnight reached **< 50° N** in geomagnetic latitude.

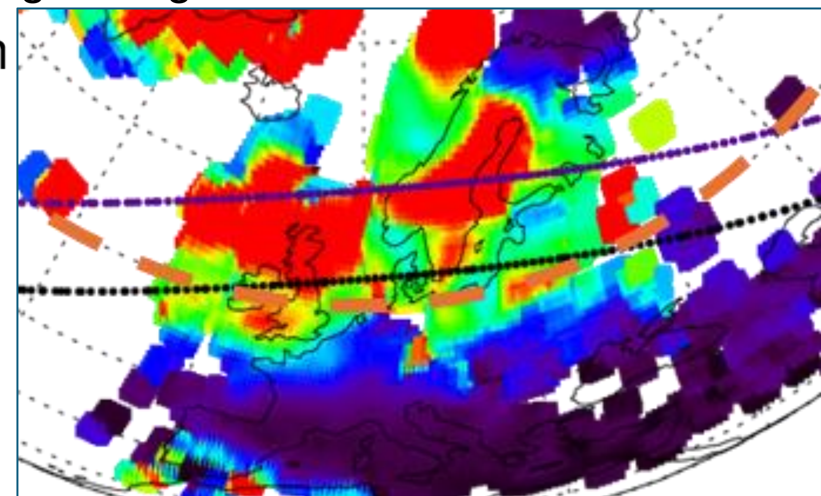

We need more investigation of the statistical analysis for the different intensity storms to reproduce the extreme observational result.

Appendix

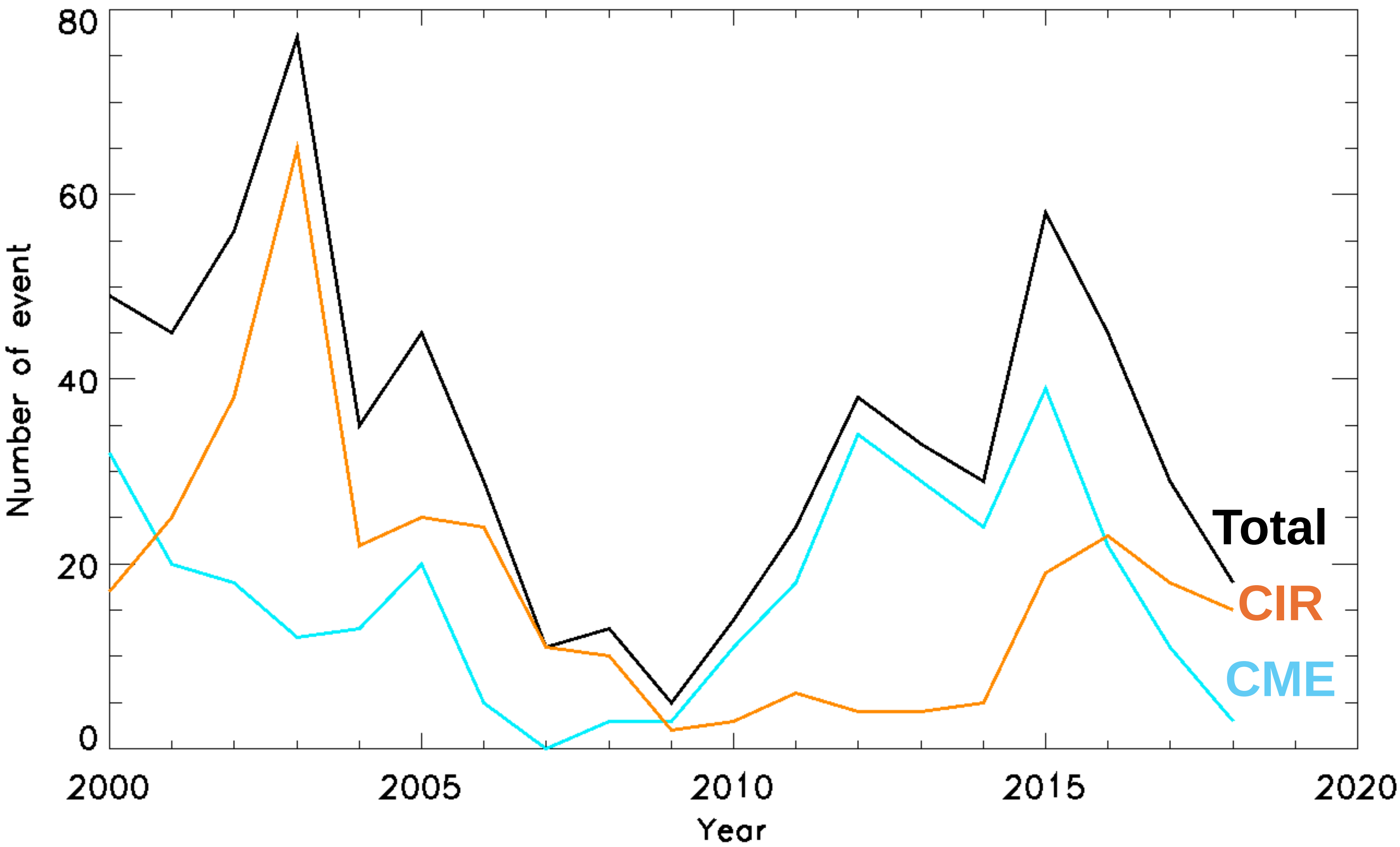
80
60
40
20
0
Number of event
2000
2005
2010
2015
2020
Year
Total
CIR
CME

Spatiotemporal variations of median ROTI at high latitudes

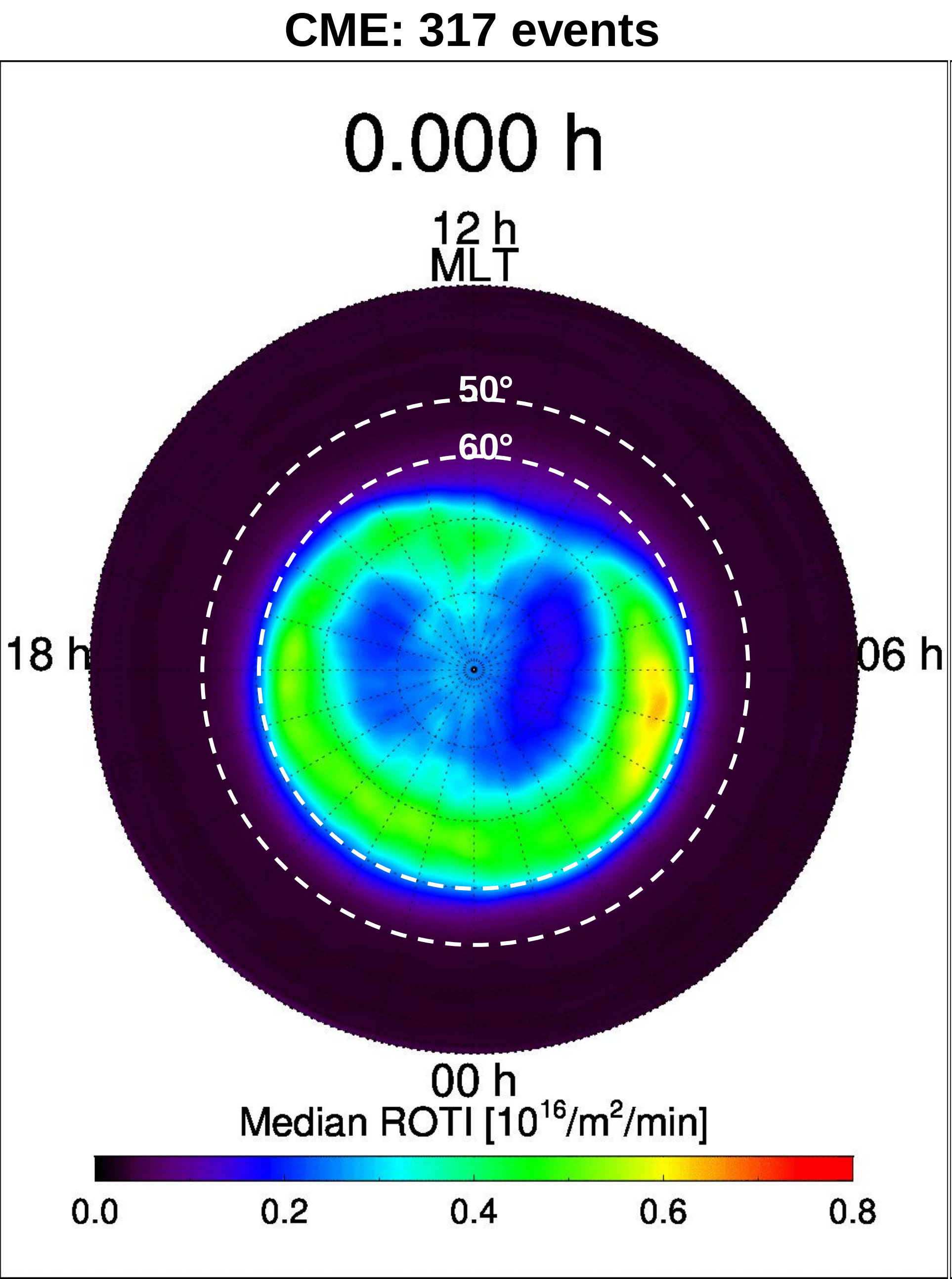

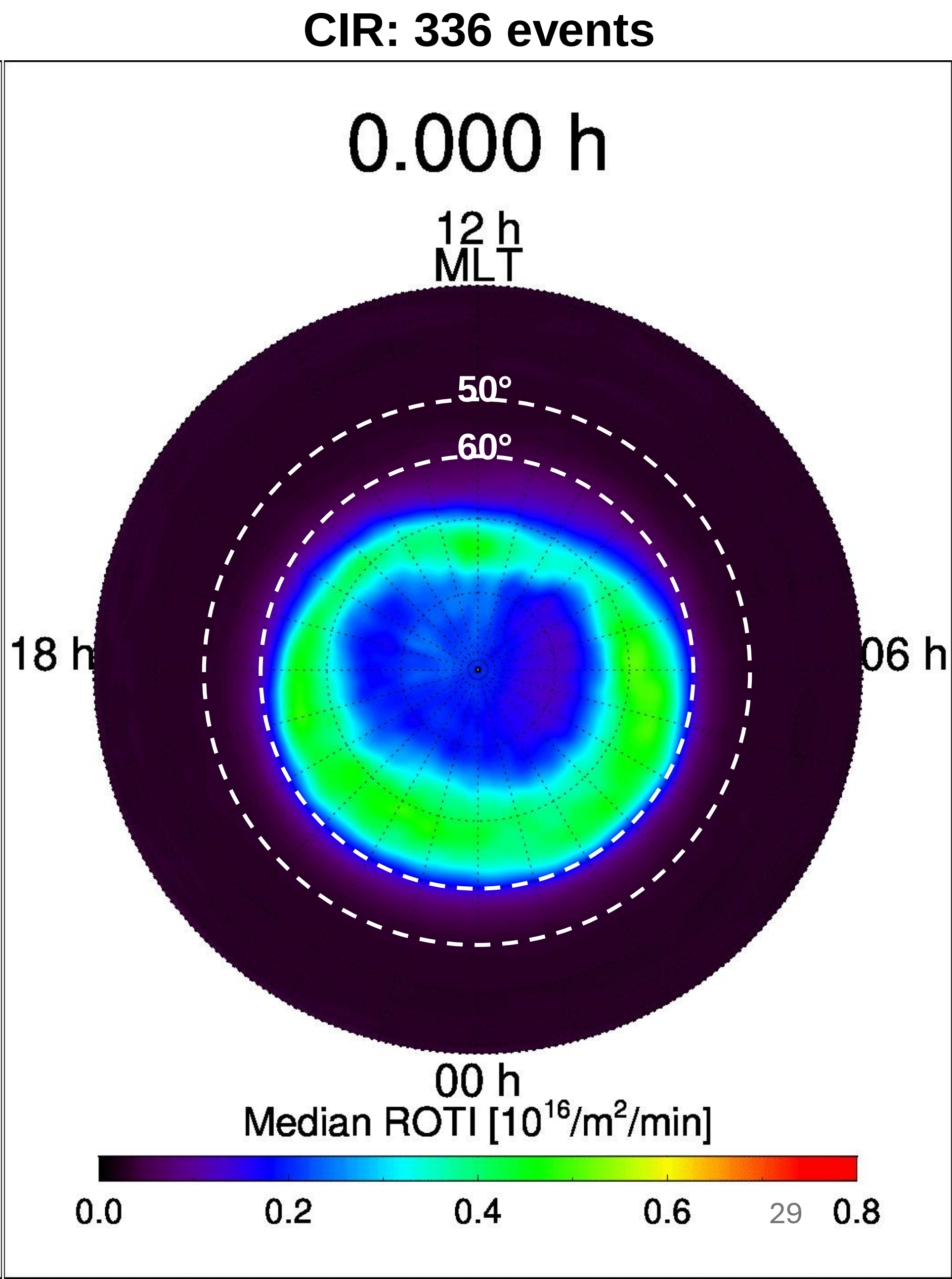

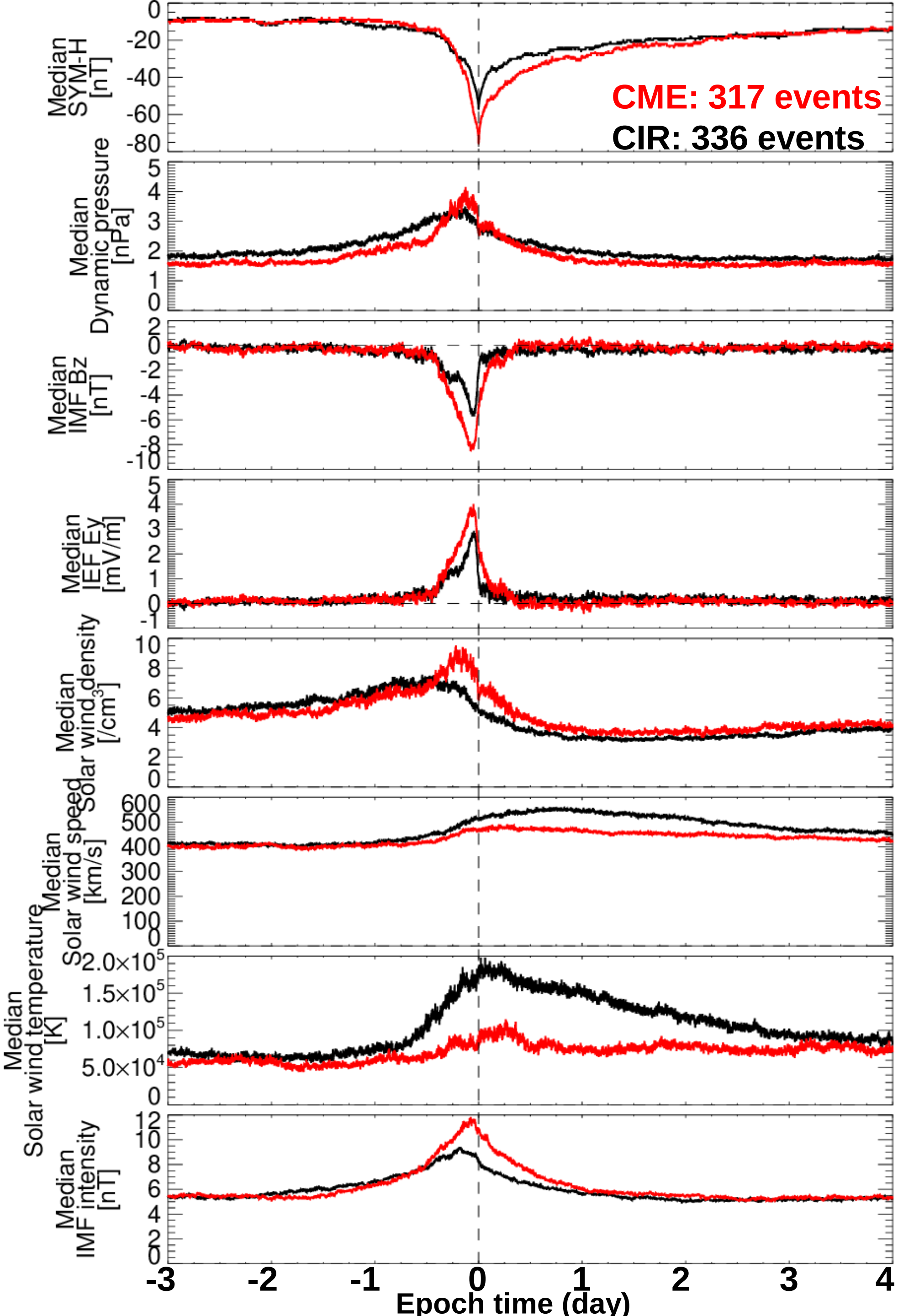
CME: 317 events
CIR: 336 events
Median SYM-H [nT]
Median Dynamic pressure [nPa]
Median IMF Bz [nT]
Median IEF Ey [mV/m]
Median Solar wind density [/cm^3]
Median Solar wind speed [km/s]
Median Solar wind temperature [K]
Median IMF intensity [nT]
Epoch time (day)

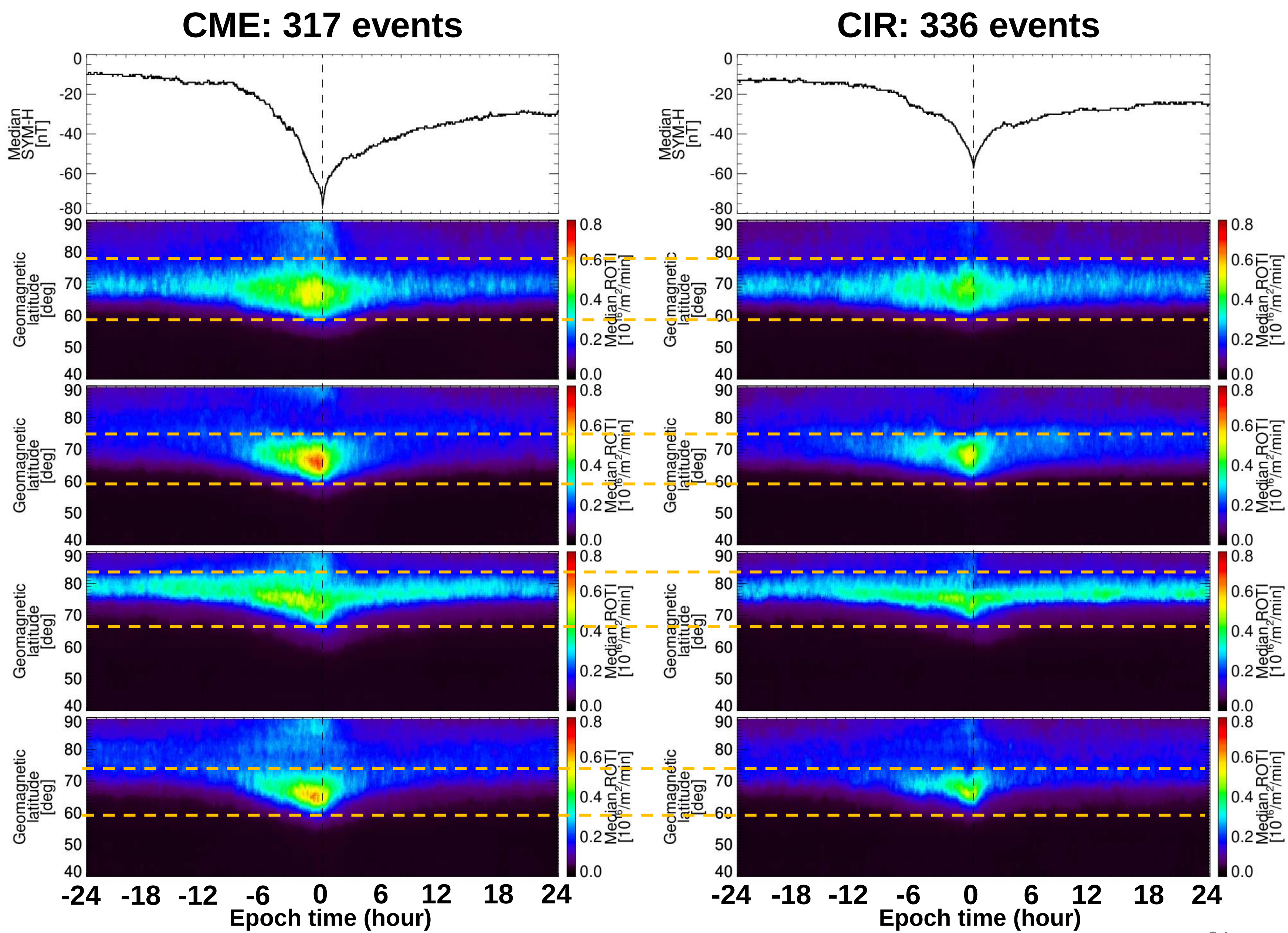

CME: 317 events
CIR: 336 events
Median SYM-H [nT]
Geomagnetic latitude [deg]
Median ROTI [10^{16}/m^2/min]
Epoch time (hour)

Spatiotemporal variations of median ROTI at high latitudes